

Characteristic Temperature Curves for Aluminum Alloys during Friction Stir Welding

An empirically derived relationship between temperature and weld energy is used to predict maximum friction stir welding temperatures in aluminum alloys

BY C. HAMILTON, S. DYMEK, AND A. SOMMERS

ABSTRACT

Review of published friction stir welding (FSW) data across numerous aluminum alloys demonstrates that a characteristic relationship between the temperature ratio (the maximum welding temperature divided by the solidus temperature of the alloy) and the energy per unit length of weld exists. When the temperature ratio is plotted as a function of the energy per unit length of weld, a linear relationship whose slope is dependent on the thermal diffusivity of the alloy is revealed. Utilizing these characteristic curves, the maximum welding temperatures were estimated for Sc-modified Al-Zn-Mg-Cu alloy extrusions joined through FSW at 225, 250, 300, and 400 rev/min (all other weld parameters held constant). The characteristic curves successfully predict the maximum weld temperatures at the lower energy weld conditions, i.e., 225 and 250 rev/min, but for the high-energy welds, 300 and 400 rev/min, the curves overpredict the maximum weld temperatures. Despite this discrepancy, the characteristic curves demonstrate that it is feasible to predict the maximum FSW temperature in an alloy if the thermal diffusivity, welding parameters, and tool geometry are known.

Introduction

Friction stir welding (FSW) is a novel solid-state joining process that is gaining popularity in the manufacturing sector and, in particular, the aerospace industry (Refs. 1, 2). Because no melting occurs during FSW, the process is performed at much lower temperatures than conventional welding techniques and circumvents many of the environmental and safety issues associated with these welding methods. The plastic deformation and temperature profile during FSW produce a microstructure characterized by a central weld nugget surrounded by a thermo-mechanically affected zone (TMAZ) and heat-affected zone (HAZ). The welded joint is fundamentally defect free and displays excellent mechanical properties when compared to conventional fusion

welds (Refs. 3, 4). Since its introduction, numerous investigations have sought to characterize the principles of FSW and to model the microstructural evolution and temperature behavior. The current status of FSW research has been well summarized by Mishra and Ma (Ref. 5).

Researchers have found success in modeling the heat transfer characteristics of FSW. For example, Frigaard et al. (Ref. 6) developed a finite difference thermal model for a moving heat source and correlated the predicted temperature profile with the measured temperature profile for friction stir welded 6082-T6 and 7108-T79 extrusions. Utilizing a visco-plastic model,

Ulysse (Ref. 7) studied the impact of varying weld parameters on the temperature distribution in 7050-T7451 plate. Also, Khandkar et al. (Refs. 8, 9) introduced a heat input model based on the torque of the FSW tool and successfully applied the model to friction stir welded aluminum 6061-T651 plate.

A commonality to each of these approaches, however, is the need to develop a computer simulation to satisfactorily solve the heat transfer equation for the alloy and welding conditions of interest, and to calculate the thermal profile and maximum welding temperature. To circumvent this sometimes work-intensive process, Roy et al. (Ref. 10) utilized the Buckingham π -Theorem and proposed a dimensionless parameter based on material properties and process parameters to predict the maximum weld temperature during friction stir welding. Colegrove et al. (Ref. 11) also pursued a technique that would predict the heat generation in aluminum alloys during FSW based solely on material properties, in particular the solidus temperature of the alloy and flow stress. Defining the “contact radius” between the tool and workpiece as a measure of heat transfer efficiency between them, their work showed good agreement between predicted and experimental temperatures when applied to 7449-T73, 2024-T3, and 6013-T6 sheets.

Through similar motivation to derive a more direct approach to predict friction stir welding temperatures in aluminum alloys, the current investigation utilizes Khandkar’s torque-based heat input model to develop a relationship between the maximum welding temperature, solidus temperature, and energy per unit length of weld. This empirically derived relationship generates temperature curves characteristic to specific thermal diffusivities that correlate the temperature ratio (the ratio of the maximum weld temperature to the solidus temperature)

KEYWORDS

Friction Stir Welding
Peak Temperature
Aluminum Alloys
Specific Energy
Thermal Modeling

C. HAMILTON (hamiltbc@muohio.edu) and A. SOMMERS are with Miami University, Department of Mechanical and Manufacturing Engineering, Oxford, Ohio. S. DYMEK is with AGH University of Science and Technology, Faculty of Metals Engineering and Industrial Computer Science, Kraków, Poland.

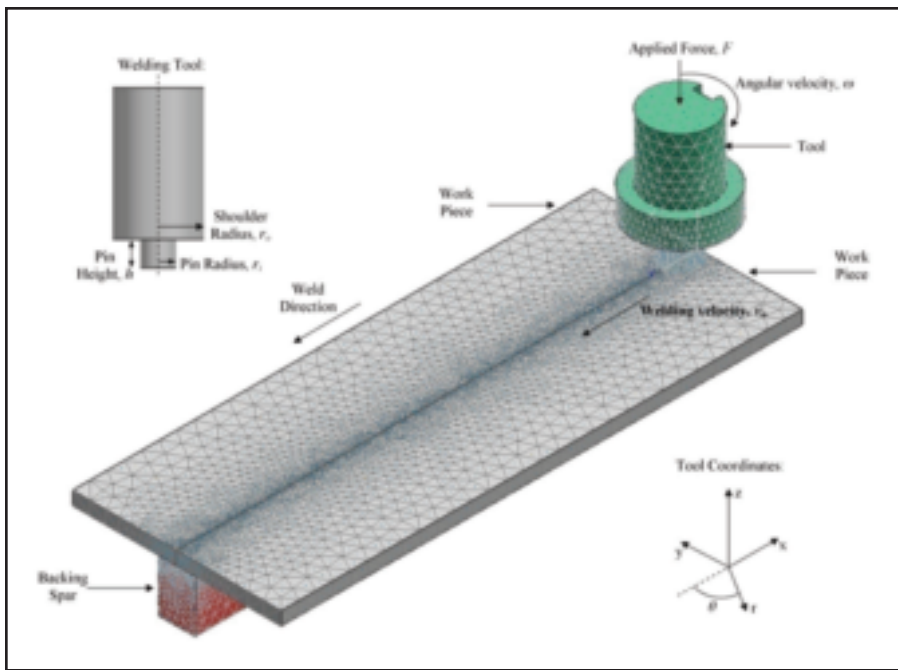


Fig. 1 — Friction stir weld configuration, tool coordinate system, and tool geometry.

with the weld energy. From these curves, the maximum welding temperature may be estimated for a given aluminum alloy if the tool geometry, welding parameters, solidus temperature, and thermal diffusivity are known.

Experimental Procedure

For this investigation, Sc-modified Al-Zn-Mg-Cu billets (SSA038) were produced by UES, Inc., through direct chill casting and then extruded as 50.4- × 6.35-mm bars. The chemical compositions of SSA038 is summarized in Table 1 along with that of aluminum 7075 for reference and comparison (Ref. 12). Following extrusion, the bars were heat treated to a-T6 temper through the following schedule: 1) solution heat treat at 460°C for one hour followed by an additional hour at 480°C, 2) rapid quench in water to room temperature, and 3) age at 120°C for 19 h. The density of SSA038 is 2820 kg/m³, and the solidus temperature is 528°C.

After heat treatment, the bars were cut into eight, 305-mm lengths and sent to the Edison Welding Institute (EWI, Columbus, Ohio) to produce four friction stir welds in the configuration represented — Fig. 1. As shown in the diagram, FSW occurs along the L direction of the extrusions with a clockwise tool rotation. The diameter of the FSW tool shoulder was 17.8 mm, the pin diameter tapered linearly from 10.3 mm at the tool shoulder to 7.7 mm at the tip, and the pin depth was 6.1 mm.

More specific details of the tool design are proprietary to EWI, but Mishra and Ma (Ref. 5) have reviewed many of the common FSW tool designs that are indicative of that utilized in this investigation. With a constant weld velocity of 2.1 mm/s and an applied force of 22 kN, unique welds were produced at the following tool rotation speeds: 225, 250, 300, and 400 rev/min. Even though the applied force during FSW was set to 22 kN, real-time data from the welding trials revealed that the load oscillated as the machine continuously corrected the load toward the set point. Consequently, the average load during welding deviated from the desired set point; therefore, the average load was determined from the recorded data for each weld condition and was utilized in the analysis of that condition. These average load values are 21.4, 20.1, 22.8, and 20.1 kN for 225, 250, 300, and 400 rev/min, respectively. The recorded data verified that the weld velocity remained constant at 2.1 mm/s for all welding trials.

By utilizing a Mikron M7815 thermal imaging camera during welding, the temperature profile across the weld was experimentally recorded for each condition. The thermal emissivity for the infrared data was calibrated by imaging an extrusion length heated to 460°C and adjusting the emissivity value until the recorded temperature of the camera matched the reference temperature. The appropriate thermal emissivity value was determined to be 0.285. The experimental tempera-

ture data were used to verify the efficacy of the characteristic curves proposed from this investigation.

Discussion

Energy per Unit Length of Weld

Because the weld velocity (v_w), tool rotation speed (ω), and applied force (F) all influence the total energy imparted to the workpieces, the total heat input more appropriately indicates the welding conditions than any individual welding parameter. The energy per unit length of weld was derived by Khandkar (Ref. 8) from a torque-based model for which the total torque, T_{total} , is expressed as the sum of torque contributions from the tool shoulder against the workpiece, bottom of the tool pin against thickness material, and pin surface against thickness material. For the FSW representation in Fig. 1, where r_o is the radius of the tool shoulder, r_{i1} is the radius of the pin at the tool shoulder, r_{i2} is the radius of the pin at the pin bottom, h is the pin height, τ is the shear stress during welding, and F is the applied force, the total torque then becomes

$$T_{total} = \int_{r_{i1}}^{r_o} (\tau r)(2\pi r) dr + \int_0^{r_{i2}} (\tau r) (2\pi r) dr + 2\pi r_i^2 h F$$

To simplify the evaluation of Equation 1, the taper of the welding pin is ignored, i.e., $r_{i1} = r_{i2}$, and defining τ as the product of the coefficient of friction between the tool and workpieces, μ , with the average pressure ($F/\pi r^2$), Equation 1 becomes

$$T_{total} = 2\mu F \left(\frac{r_o}{3} + \frac{r_i^2}{r_o^2} h \right) \quad (2)$$

The coefficient of sliding friction between aluminum and steel depends on the temperatures produced by the welding conditions. Frigaard et al. (Ref. 6) reasoned that the coefficient of friction between alu-

Table 1 — Chemical Compositions of SSA038 with 7075 as Reference

Element	Wt-%	
	SSA038	7075
Zn	7.11	5.60
Mg	2.14	2.50
Cu	1.56	1.60
Mn	0.25	0.30
Zr	0.17	< 0.05
Sc	0.38	—
Cr	< 0.05	0.23
Ti	< 0.05	0.20
other, each	0.35	1.03
Al	Balance	

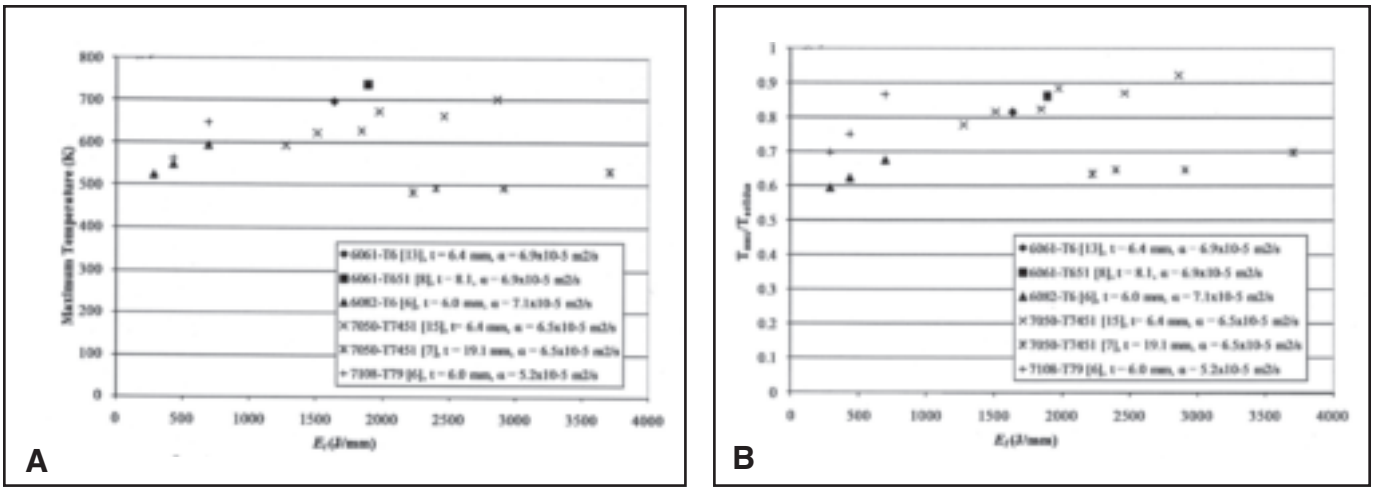


Fig. 2 — A — Maximum temperature as a function of energy per weld length; B — temperature ratio as a function of energy per weld length.

Table 2 — Energy per Unit Length of Weld and Measured Maximum Temperature

Alloy	Tool Geometry			Rev/Min	Welding Parameters			Measured Max. T (K)				
	r _O (mm)	r _I (mm)	h (mm)		v _w (mm/s)	F (kN)	E (J/mm)					
AA7108-T79 (Ref. 6)	7.5	2.5	6.0	1500	5.0	7	696	648				
				1500	8.0	7	435	563				
				1500	12.0	7	290	523				
				180	0.85	20	1845	628				
AA6061-T6 (Ref. 11)	12.0	9.5	6.0	344	2.2	13	1639	698				
				390	2.4	22	1896	739				
					7.5	2.5	6.0	1500	5.0	7	696	594
					1500	8.0	7	435	548			
AA6082-T6 (Ref. 6)	7.5	2.5	6.0	1500	8.0	7	435	548				
				1500	12.0	7	290	523				
				180	1.3	25	1513	623				
				180	1.7	28	1273	593				
AA7050-T7451 (Ref. 15)	10.2	3.6	6.1	360	1.7	24	1978	673				
				540	2.5	34	2464	663				
				810	3.8	39	2868	703				
				AA7050-T7451 (Ref. 7)	9.5	3.2	6.4	490	1.4	20	2916	493
700	1.0	13	3710					533				
700	1.9	16	2403					493				
700	2.6	18	2229					483				

minum and mild steel should be set as the average value between 0.5 for sticky friction and 0.25 for dry sliding, while Soundararajan et al. (Ref. 13) allowed μ to vary between 0.5 and 0.4 depending on the welding conditions. For this investigation, initial calculations of the energy used a coefficient of friction of 0.5; however, if energy levels exceeded 2000 J/mm, i.e., “hot” welding conditions, the coefficient of friction was reduced to 0.45, and if the energies levels exceeded 3000 J/mm, the coefficient of friction was further reduced

to 0.4. The energies were then recalculated according to the reassigned value of μ . The energy per unit length of weld, E_l , is found by dividing the average power, P_{avg} , by the weld velocity to yield the expression in Equation 3.

$$E_l = \frac{P_{avg}}{v_w} = T_{total} \frac{\omega}{v_w} \quad (3)$$

This formulation of weld energy does not take into account heat generation due to plastic deformation. In the review paper by Nandan et al. (Ref. 14), the difficulties

of estimating the coefficient of friction during FSW are discussed, and thermal models that include volumetric heating by visco-plastic dissipation are presented.

Survey of Data from the Literature

A survey of the friction stir welding literature on thermal modeling of aluminum alloys produced the information presented in Tables 2 and 3. These specific investigations were selected because the researchers experimentally measured the

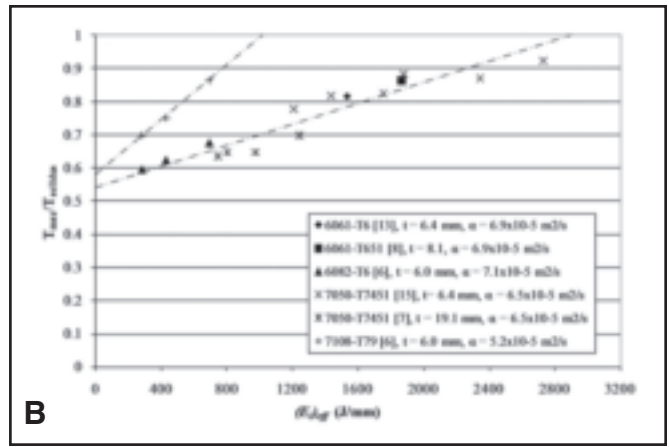
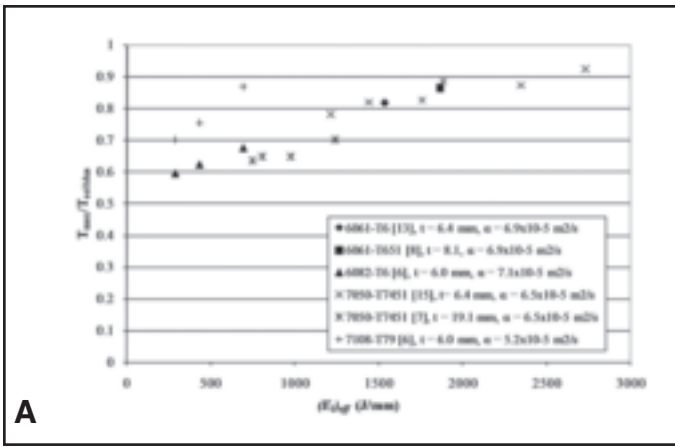


Fig. 3 — A — Temperature ratio as a function of effective energy per weld length; B — with linear regression curves added.

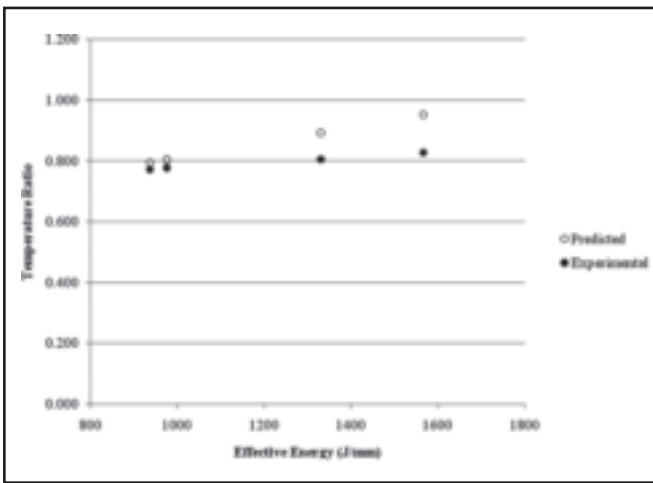


Fig. 4 — Experimental and predicted temperature ratio as a function of effective energy per weld length for SSA038-T6.

temperature profile to verify their thermal model and included the welding parameters and tool geometry, such that energy per unit length calculations could be made for their particular weld conditions (Table 2). Force values taken from Ref. 7 are numerical predictions, not experimental observations, for the weld velocity and tool rotation speed combinations.

Table 3 displays the properties for the investigated alloys at room temperature, where ρ is the density, c_p is the heat capacity, k is the thermal conductivity, and α is the thermal diffusivity of the alloy ($\alpha = k/c_p\rho$). Though the heat capacity and thermal conductivity are temperature-dependent properties, a goal of this work is to predict friction stir welding temperatures utilizing these material properties at room temperature. Also listed in Table 3 are the maximum temperatures recorded by each

researcher during welding. Though the thermocouple locations from each study are not identical, these temperatures are assumed to be the true maximum temperatures, i.e., temperatures under the tool shoulder, as each investigator did attempt to record the temperature near the weld centerline.

Figure 2A plots the experimentally measured maximum temperature, T_{max} , as a function of the energy per length of weld, E_l , for the data in Table 2. The correlation between the two parameters from each data set is

self-evident because the energy per length of weld must also reflect the maximum achievable temperature, i.e., as the welding energy increases, so must the welding temperature. As seen in the figure, the data tend to group based on alloy type and product thickness. Thus, the maximum temperatures for the 6061 and 6082 alloys with similar thicknesses (6.0, 6.4, and 8.13 mm), show the same linear relationship with E_l , while the two 7050 data sets with different product thicknesses (6.4 and 19.1 mm) display unique relationships between temperature and energy.

Because 6061 and 6082 share a similar chemistry and thickness, the common relationship between temperature and energy is expected. Despite 7050 having a distinct chemistry from the 6XXX alloys, its thermal diffusivity ($6.5 \times 10^{-5} \text{ m}^2/\text{s}$) is

comparable to both 6061 and 6082 (6.9 and $7.1 \times 10^{-5} \text{ m}^2/\text{s}$, respectively); therefore, for the same thickness, the 7050 data from Reynolds's (Ref. 15) investigation would be expected to show a similar temperature/energy trend as that of 6061 and 6082. Though showing a similar slope to that of 6061 and 6082, the 7050 relationship in Fig. 2A is shifted to the right, indicating that lower maximum temperatures are produced in 7050 at the same energy levels.

Consider, however, that as the welding temperature approaches the solidus temperature, T_s , of an alloy, the material will soften, slip will occur, and less energy will be transferred into the workpiece. The solidus temperatures of 6061 and 6082 are greater than that of 7050; therefore, under the same welding conditions, the transfer of energy between the tool and the workpiece is more efficient in the 6XXX alloys than in 7050. Hence, the maximum temperature for a given energy level will increase with increasing solidus temperature. Figure 2B demonstrates that when the temperature ratio, T_{max}/T_s , is plotted as a function of E_l , the data group according to thermal diffusivity and product thickness. The data sets from 6061, 6082, and Reynolds's 7050 display a relationship distinct from 7108, which has a lower thermal diffusivity, and from Ulysse's 7050, which has a greater product thickness.

Consider a welding condition for which the initial material thickness approaches the length of the tool pin. As the workpiece thickness increases relative to the pin length, material below the pin conducts more heat away from the process zone. As the material thickness continues to increase, additional heat conduction will diminish until a threshold thickness is reached beyond which greater and greater workpiece thicknesses will effectively conduct the same amount of heat away from

Table 3 — Room Temperature Alloy Data from Survey of Literature

Alloy	Thick (mm)	ρ (kg/m ³)	c_p (J/kg·K)	k (W/m·K)	$\alpha \times 10^{-5}$ (m ² /s)	Solidus Temp. (K)	Ref.
AA7108-T79	6.0	2780	960	140	5.2	748	Frigaard (Ref. 6)
AA6061-T6	6.4	2700	896	167	6.9	855	Soundararajan (Ref. 13)
AA6061-T651	8.13	2700	896	167	6.9	855	Khandkar (Ref. 8)
AA6082-T6	6.0	2700	889	170	7.1	879	Frigaard (Ref. 6)
AA7050-T7451	6.4	2830	860	157	6.5	761	Reynolds (Ref. 15)
AA7050-T7411	19.1	2830	860	157	6.5	761	Ulysse (Ref. 7)

the process zone. Below this threshold thickness and for a given alloy and FSW tool, the maximum welding temperature at a specific energy level will decrease as the material thickness increases. To account for the influence of material thickness below the threshold value, a scaling parameter, β , is defined as the ratio of the pin length, h , to the product thickness, t . The effective energy per weld length, $(E_l)_{eff}$, then becomes the energy per weld length multiplied by the scaling factor, such that

$$(E_l)_{eff} = \frac{h}{t} E_t = \beta E_t \quad (4)$$

Assuming that the FSW data in Tables 2 and 3 are within the range that the scaling factor would be applicable, Fig. 3A plots T_{max}/T_s as a function of $(E_l)_{eff}$, and Ulysse's 7050 data now reveal the same temperature ratio/energy relationship as the 6061, 6082, and Reynolds's 7050 data. The distinction between this relationship and that of 7108 lies in the difference between the thermal diffusivities of the data sets. The thermal diffusivity of 7108 is 5.2×10^{-5} m²/s, while that of the 6XXX and 7050 data set is approximately 6.75×10^{-5} m²/s (though specific diffusivities are either slightly higher or lower than this value).

The temperature ratio of the 7108 data set shows greater sensitivity to $(E_l)_{eff}$, i.e., for equivalent increases in energy level, the maximum temperature increases more quickly for 7108 than for 6XXX and 7050. As thermal diffusivity decreases, the ability of an alloy to conduct energy away from a heat source also decreases. If the maximum temperature during FSW occurs under the tool shoulder, which is also the principal source of heat, then for a fixed tool material and energy level, the maximum temperature at this location must increase in alloys with lower thermal diffusivities if all other boundary conditions remain constant. Higher temperature ratios, therefore, are produced in 7108 at equivalent $(E_l)_{eff}$ than those produced in 6XXX or 7050.

Figure 3B displays the temperature

Table 4 — Effective Total Energies and Maximum Weld Temperatures for Each Weld Condition

Rev/Min	$(E_l)_{eff}$ (J/mm)	Maximum Welding Temperature (°C)	
		Experimental	Predicted
225	938	346	363
250	977	350	371
300	1331	372	442
400	1567	390	490

ratio/energy level data with linear regressions added to each data set. Both regressions converge near the same T_{max}/T_s ratio for an energy level of zero, the 7108 data set intercepting the axis at 0.58 and the 6XXX and 7050 data set intercepting the axis at 0.54. Though each regression converges at approximately the same intercept, it is difficult to rationalize any physical significance to this point, i.e., the temperature ratio at zero weld energy, other than as a convenient mathematical construct. The relationship between the temperature ratio and energy, however, does hold over the region of practical welding conditions. If the intercept value is taken as 0.56, then an empirical relationship between the temperature ratio and effective energy level is developed that is applicable to each of the aluminum alloys

$$\frac{T_{max}}{T_s} = m_\alpha (E_l)_{eff} + 0.56 \quad (5)$$

where m_α is the slope of the linear relationship, and the α subscript indicates a dependence on the thermal diffusivity of the alloy. If the relationship between the slope and α is interpolated with the given experimental data, then Equation 5 may be rewritten as

$$\frac{T_{max}}{T_s} = (0.0013 - 16.5\alpha)(E_l)_{eff} + 0.56 \quad (6)$$

Equation 6 describes a relationship between the welding energy and maximum welding temperature that is characteristic across numerous aluminum alloys. If the

thermal properties and solidus temperature for a given aluminum alloy are known, then the maximum welding temperature during FSW may be estimated from the welding parameters, workpiece thickness, and tool geometry utilizing Equation 6.

Application to SSA038-T6 Data

Utilizing the empirical relationship in Equation 6, the maximum temperature for each SSA038-T6 weld condition can be predicted. Table 4 summarizes these predicted temperatures and the experimental temperatures recorded for each weld trial. At 225 rev/min, the characteristic curve predicts a maximum temperature of 363°C, a 5% error with respect to the experimental value. A similar success is seen at 250 rev/min for which the characteristic curve predicts a maximum temperature of 371°C, only a 6% error. The accuracy of these lower energy results compare favorably with the accuracy of the models proposed by Roy et al. (Ref. 10) and Colegrove et al. (Ref. 11). The dimensionless parameter approach by Roy predicted temperatures to within 10–15% of the experimental temperatures, while the model of Colegrove predicted temperatures easily within 10% of the actual welding temperature, but often were as accurate as $\pm 5^\circ\text{C}$ of the experimental values.

For the higher energy welds, however, the efficacy of this model decreases. At 300 and 400 rev/min, the error in the predicted temperature is 19 and 26%, respectively. Figure 4 plots the temperature ratio as a function of the effective energy for the

experimental temperature data and predicted temperature data and reveals the discrepancy between the two relationships as the welding energy increases. Clearly, Equation 6 assumes a slope that is steeper than that of the actual relationship. As such, the predicted and experimental temperatures show relatively good agreement below 1100 J/mm, but diverge as the effective energy increases. The inability of Equation 6 to adequately capture the temperatures at higher weld energies lies in the interpolation of m_α from Equation 5. As previously discussed, m_α represents the thermal diffusivity-dependent slope of the temperature ratio/effective energy relationship. The expression for m_α introduced into Equation 6 models the data for both 7108, a "low" thermal diffusivity alloy, and from 6XXX and 7050, "high" diffusivity alloys. Thus, when Equation 6 is applied, it will underestimate the slope for alloys with thermal diffusivities similar to 7108, but overestimate the slope for alloys with thermal diffusivities similar to 6XXX and 7050. Because SSA038 shares a similar chemistry to 7050, the thermal diffusivities would be expected to be similar, and Equation 6 will overestimate the slope of the characteristic curve for SSA038.

Conclusions

Based on the torque during friction stir welding, the energy per unit length of weld was calculated for numerous investigations on various aluminum alloys. The data revealed a characteristic linear relationship between the temperature ratio, maximum welding temperature divided by the solidus temperature of the alloy, and effective energy per length of weld. The thermal diffusivity of the alloy determined the slope, and from this relationship, an empirical formula was proposed that can be used to estimate the maximum welding temperature from the tool geometry, welding parameters, solidus temperature, and thermal diffusivity for any given aluminum alloy. Using this empirical relationship, the maximum welding temperatures were estimated for SSA038-T6 (a Sc-modified Al-Zn-Mg-Cu aluminum alloy) extrusions joined at four different rotation speeds. For welding energies less than 1100 J/mm, the predicted temperatures from the characteristic curves showed good agreement with the experimental data; however, above this energy level, the predicted temperatures diverged from the experimental values.

The discrepancy between the two relationships rests in the interpolation of the slope of the characteristic curve as it relates to the thermal diffusivity. For thermal diffusivities similar to AA7108 (the lower limit of this investigation), the model will underestimate the slope of the

characteristic curve, but for thermal diffusivities on the order of 6XXX or 7050 (the upper limit of this investigation), the model overestimates the slope of this relationship. Despite the discrepancy, the characteristic curves demonstrate the possibility of predicting the maximum FSW temperature from the thermal diffusivity, welding parameters, and tool geometry.

Acknowledgments

The authors acknowledge the Polish Ministry of Science and Higher Education (Grant No. N507 446 337), UES, Inc., and the Materials and Manufacturing Directorate at Wright-Patterson AFB for their support of this research.

References

1. Thomas, W. M., et al. Dec. 1991. Great Britain Patent Application No. 9125978.8.
2. Dawes, C., and Thomas, W. Nov./Dec. 1995. *TWI Bulletin* 6: 124.
3. Sutton, M. A., Yang, B. C., Reynolds, A. P., and Yan, J. H. 2004. Banded microstructure in 2024-T351 and 2524-T351 aluminum friction stir welds. *Material Science and Engineering A* 364: 66–74.
4. Hamilton, C., Dymek, S., and Blicharski, M. 2007. Comparison of mechanical properties for 6101-T6 extrusions welded by friction stir welding and metal inert gas welding. *Archives of Metallurgy and Materials* 52: 67–72.
5. Mishra, R. S., and Ma, Z. Y. 2005. Friction stir welding and processing. *Material Science and Engineering R* 50: 1–78.
6. Frigaard, O., Grong, O., and Midling, O. T. 2001. A process model for friction stir welding of age hardening aluminum alloys. *Metallurgical and Materials Transactions A* 32(5): 1189–1200.
7. Ulysse, P. 2002. Three-dimensional mod-

eling of the friction stir-welding process. *International Journal of Machine Tools and Manufacture* 42: 1549–1557.

8. Khandkar, M. Z. H., Khan, J. A., and Reynolds, A. P. 2003. Predictions of temperature distribution and thermal history during friction stir welding: Input torque based model. *Science and Technology of Welding and Joining* 8(3): 165–174.

9. Khandkar, M. Z. H., Khan, J. A., Reynolds, A. P., and Sutton, M. A. 2006. Predicting residual thermal stresses in friction stir welded metals. *Journal of Materials Processing Technology* 174: 195–203.

10. Roy, G. G., Nandan, R., and DebRoy, T. 2006. Dimensionless correlation to estimate peak temperature during friction stir welding. *Science and Technology of Welding and Joining* 11: 606–608.

11. Colegrove, P. A., Shercliff, H. R., and Zettler, R. 2007. Model for predicting heat generation and temperature in friction stir welding from material properties. *Science and Technology of Welding and Joining* 12: 284–297.

12. Senkova, S. V., Senkov, O. N., and Miracle, D. B. 2006. Cryogenic and elevated temperature strengths of an Al-Zn-Mg-Cu alloy modified with Sc and Zr. *Metallurgical and Materials Transactions A* 37(12): 3569–3575.

13. Soundararajan, V., Zekovic, S., and Kovacevic, R. 2005. Thermo-mechanical model with adaptive boundary conditions for friction stir welding of Al AA6061. *International Journal of Machine Tools and Manufacture* 45: 1577–1587.

14. Nandan, R., DebRoy, T., and Bhadeshia, H. K. D. H. 2008. Recent advances in friction-stir welding — Process, weldment structure and properties. *Progress in Materials Science* 53: 980–1023.

15. Reynolds, A. P., Tang, W., Khandkar, Z., Khan, J. A., and Lindner, K. 2005. Relationships between weld parameters, hardness distribution and temperature history in Alloy 7050 friction stir welds. *Science and Technology of Welding and Joining* 10: 190–199.

An Important Event on Its Way?

Send information on upcoming events to the Welding Journal Dept., 550 NW LeJeune Rd., Miami, FL 33126. Items can also be sent via FAX to (305) 443-7404 or by e-mail to woodward@aws.org.

Dear Readers:

The *Welding Journal* encourages an exchange of ideas through letters to the editor. Please send your letters to the Welding Journal Dept., 550 NW LeJeune Rd., Miami, FL 33126. You can also reach us by FAX at (305) 443-7404 or by sending an e-mail to Kristin Campbell at kcampbell@aws.org.